

LA-UR-21-22104 (Accepted Manuscript)

Subtropical Eastern North Pacific SST Bias in Earth System Models

Balaguru, Karthik
Van Roekel, Luke
Leung, L. Ruby
Veneziani, Carmela

Provided by the author(s) and the Los Alamos National Laboratory (2021-09-27).

To be published in: Journal of Geophysical Research: Oceans

DOI to publisher's version: 10.1029/2021JC017359

Permalink to record: <http://permalink.lanl.gov/object/view?what=info:lanl-repo/lareport/LA-UR-21-22104>

Disclaimer:

Los Alamos National Laboratory, an affirmative action/equal opportunity employer, is operated by Triad National Security, LLC for the National Nuclear Security Administration of U.S. Department of Energy under contract 89233218CNA000001. By approving this article, the publisher recognizes that the U.S. Government retains nonexclusive, royalty-free license to publish or reproduce the published form of this contribution, or to allow others to do so, for U.S. Government purposes. Los Alamos National Laboratory requests that the publisher identify this article as work performed under the auspices of the U.S. Department of Energy. Los Alamos National Laboratory strongly supports academic freedom and a researcher's right to publish; as an institution, however, the Laboratory does not endorse the viewpoint of a publication or guarantee its technical correctness.

14 **Abstract**

15 This study systematically evaluates the warm SST bias in the Subtropical Eastern North
 16 Pacific (SENP), a problem plaguing most CMIP6 models, using the Energy Exascale Earth
 17 System Model version 1 (E3SM). Compared to the model at its standard resolution (1°
 18 atmosphere, 30-60 km ocean), the SST bias improves in several regions at high resolu-
 19 tion (0.25° atmosphere, 18-6 km ocean) except in subtropical eastern boundary regions,
 20 such as the SENP. A mixed layer heat budget analysis reveals that errors in the surface
 21 radiative fluxes and horizontal heat advection are primarily responsible for the bias. Anal-
 22 ysis of HighResMIP models indicates that the lack of improvement in the SENP SST
 23 bias with resolution is not native to E3SM alone. A larger CMIP6 inter-model correla-
 24 tion of SST bias with biases in surface winds than radiation highlights the important role
 25 of large-scale circulation biases in the SENP SST bias in coupled models.

26 **Plain Language Summary**

27 Most coupled climate models suffer from warm sea surface temperature (SST) bi-
 28 ases near subtropical eastern boundary regions in the global oceans. Despite numerous
 29 improvements in models over time, these problems have persisted. While several previ-
 30 ous studies focused on understanding the bias in the Southeast Atlantic and Southeast
 31 Pacific, a systematic evaluation of the bias for the Subtropical Eastern North Pacific (SENP)
 32 region has not been performed. In this study, we address this issue using fully-coupled
 33 and forced simulations, at different resolutions, based on the Energy Exascale Earth Sys-
 34 tem Model version 1 (E3SM). Compared to the model at its standard resolution (1° at-
 35 mosphere, 30-60 km ocean), the SENP SST bias does not improve significantly at high
 36 resolution (0.25° atmosphere, 18-6 km ocean). Analysis reveals that errors in surface ra-
 37 diative fluxes due to misrepresentation of stratus clouds, and errors in horizontal heat
 38 advection associated with biases in surface winds are primarily responsible for the SENP
 39 SST bias. Finally, the behavior noted in E3SM can also be extended to other climate
 40 models, highlighting the broad nature of these results and the important role of large-
 41 scale circulation biases in the SENP bias in coupled models.

42 **1 Introduction**

43 The subtropical eastern boundary regions in the global oceans play a key role in
 44 the climate of the earth system. These are regions with shallow marine stratocumulus
 45 cloud decks that modulate the planet's greenhouse gas forcing, and consequently, the ra-
 46 diative balance (Richter, 2015). Stratus clouds are maintained partly by cold sea sur-
 47 face temperatures (SSTs) associated with the equatorward flowing eastern boundary cur-
 48 rents that form the eastern branch of subtropical gyres (Kessler, 2006). Also, these cur-
 49 rents induce Ekman divergence along the coast (Bakun & Nelson, 1991), causing the up-
 50 welling of cold nutrient-rich waters making these regions some of the most biologically
 51 productive globally (Chavez & Messié, 2009). This makes modeling of these processes
 52 really important not only for improving our understanding of them but also to accurately
 53 project their response under climate change (Richter, 2015; Ashfaq et al., 2011; García-
 54 Reyes et al., 2015).

55 However, most coupled climate models incorrectly simulate various processes oc-
 56 curring in these regions and suffer from warm SST biases (Richter, 2015). Misrepresen-
 57 tation of stratocumulus clouds has been identified as one of the primary reasons for this
 58 bias. Model inability to produce stratocumulus decks can lead to absorption of exces-
 59 sive shortwave radiation in the upper-ocean and anomalously warm SSTs, which in turn
 60 induces a positive feedback to the initial error (Richter, 2015; Zuidema et al., 2016). Fur-
 61 ther, model resolution and errors in surface winds could also play a role through their
 62 impact on turbulent fluxes, coastal upwelling and offshore Ekman transport. (Gent et
 63 al., 2010; Richter, 2015; Zuidema et al., 2016; Richter et al., 2016; J. Ma et al., 2019).

64 Several previous studies examined the processes responsible for warm SST biases near
 65 eastern boundaries. However, they predominantly focused on the African coast in the
 66 Southeast Atlantic (Richter & Xie, 2008; Balaguru et al., 2012; Xu, Chang, et al., 2014;
 67 Xu, Li, et al., 2014; Small et al., 2015; Harlaß et al., 2018; Kurian et al., 2021) and the
 68 South American coast in the Southeast Pacific (Xie et al., 2007; Zheng et al., 2011; J. Ma
 69 et al., 2019; da Silveira et al., 2019), prompting the need for an evaluation of the bias
 70 in the Subtropical Eastern North Pacific (SENP) region.

71 To this end, we performed a suite of numerical experiments with the Energy Ex-
 72 ascale Earth System Model (E3SM) (Golaz et al., 2019) to further understand the pro-
 73 cesses responsible for warm SST biases in the SENP region. Both coupled and uncou-
 74 pled simulations, at the standard and high-resolutions, are used. A mixed-layer heat bud-
 75 get analysis is performed to understand the relative contribution of various processes to
 76 the bias. Finally, to understand the broad applicability of these results, we perform an
 77 analysis of multiple models from the Coupled Model Intercomparison Project Phase 6
 78 (CMIP6), including models in HighResMIP with both low- and high-resolution simula-
 79 tions. The main questions we want to address through this analysis are: What processes
 80 are responsible for the SENP SST bias in E3SM? Does the bias improve with model spa-
 81 tial resolution? Does the behavior of SENP SST bias found in E3SM occur in other mod-
 82 els? The rest of the paper is organized as follows. Data, model simulations and calcu-
 83 lations are described in section 2. Results are presented in section 3 and finally, a dis-
 84 cussion of the main conclusions is provided in section 4.

85 2 Methods

86 2.1 Data

87 NOAA monthly mean optimum interpolation SST analysis (Reynolds et al., 2002),
 88 obtained for the period 1980-2014 from [https://psl.noaa.gov/data/gridded/data](https://psl.noaa.gov/data/gridded/data.noaa.oisst.v2.highres.html)
 89 [.noaa.oisst.v2.highres.html](https://psl.noaa.gov/data/gridded/data.noaa.oisst.v2.highres.html), are used to compute the mean observed SST. Monthly
 90 mean SST and meridional wind stress from 24 different climate models belonging to CMIP6
 91 (Meinshausen et al., 2017) are obtained from [https://esgf-node.llnl.gov/projects/](https://esgf-node.llnl.gov/projects/esgf-llnl/)
 92 [esgf-llnl/](https://esgf-node.llnl.gov/projects/esgf-llnl/) and used to examine model biases in SST and meridional winds in the SENP
 93 region. While NOAA SST is used to compute model SST bias, the bias in meridional
 94 winds are computed based on ECMWF ORAS5 (Zuo et al., 2019) monthly mean merid-
 95 ional wind stress obtained for the same period from [https://www.ecmwf.int/en/forecasts/](https://www.ecmwf.int/en/forecasts/dataset/ocean-reanalysis-system-5)
 96 [dataset/ocean-reanalysis-system-5](https://www.ecmwf.int/en/forecasts/dataset/ocean-reanalysis-system-5). We also obtain top-of-atmosphere upwelling clear-
 97 sky shortwave radiation and the top-of-atmosphere upwelling all-sky radiation to calcu-
 98 late the shortwave cloud radiative effect (SWCRE) in different models. The SWCRE anoma-
 99 lies in models are estimated with respect to CERES-EBAF Ed4.0 observations (Loeb et
 100 al., 2009), obtained from <https://ceres.larc.nasa.gov>. Monthly mean SST data are
 101 also obtained from 8 models belonging to HighResMIP (Haarsma et al., 2016). These
 102 data, at both high and low-resolution model configurations, are used to determine if the
 103 effect of resolution on SENP SST bias in E3SM occurs in other models. 35-years (1980-
 104 2014) of output from a single ensemble member realization of a historical simulation are
 105 used for each model. The list of various models used is provided in the supplement (Ta-
 106 ble S1).

107 OAFflux monthly mean objectively analyzed air-sea fluxes (Yu & Weller, 2007) for
 108 the period 1984-2009, obtained from <http://oafux.who.edu>, are used to compute the
 109 role of surface fluxes in the mixed layer heat budget analysis for the SENP region. Grid-
 110 ded monthly mean ocean temperature and salinity based on Argo floats (Roemmich et
 111 al., 2009), obtained from [http://apdrc.soest.hawaii.edu/projects/Argo/data/gridded/](http://apdrc.soest.hawaii.edu/projects/Argo/data/gridded/On_standard_levels/index-1.html)
 112 [On_standard_levels/index-1.html](http://apdrc.soest.hawaii.edu/projects/Argo/data/gridded/On_standard_levels/index-1.html) for the period 2005-2019, are combined with OS-
 113 CAR 5-day mean ocean surface currents (Dohan & Maximenko, 2010), obtained from
 114 https://podaac.jpl.nasa.gov/dataset/OSCAR_L4_OC_third-deg for the same period,

115 to estimate the temperature time and horizontal advection tendency terms. Note that
 116 the OSCAR product provides currents averaged over the upper-30 m of the ocean and
 117 we approximate them as the mixed layer-averaged velocities. Note that there are differ-
 118 ences in periods for various products used to estimate the observed mixed layer heat bud-
 119 get. However, a similar mixed layer heat budget based on SODA3 ocean reanalysis (not
 120 shown) reveals that the differences in periods do not have a significant impact and our
 121 estimates are robust. We obtained AVISO monthly mean multi-satellite merged sea level
 122 anomalies for the period 1993-2009 from [https://www.aviso.altimetry.fr/en/home](https://www.aviso.altimetry.fr/en/home.html)
 123 [.html](https://www.aviso.altimetry.fr/en/home.html) to estimate the observed eddy kinetic energy in the ocean. The altimeter prod-
 124 ucts were produced by the CLS Space Oceanography Division as part of the Environ-
 125 ment and Climate EU ENACT project (EVK2-CT2001-00117) and with support from
 126 CNES.

127 2.2 Model

128 We performed and analyzed fully-coupled and uncoupled simulations using version
 129 1 of E3SM (Leung et al., 2020). Simulations at both the low and high-resolutions are
 130 used. The standard resolution configuration of the model (E3SM_LR) has a horizontal
 131 resolution of approximately 1° in the atmosphere with 72 vertical levels. The ocean com-
 132 ponent has a spatial resolution varying between 30 and 60 km with 60 vertical levels and
 133 a top layer thickness of 10 m (Golaz et al., 2019). In the high resolution configuration (E3SM_HR),
 134 the horizontal resolution increases to approximately 0.25° in the atmosphere. The ocean
 135 component of the E3SM_HR has a horizontal resolution varying between 18 and 6 km
 136 with 80 vertical levels and a top layer thickness of 2 m (Caldwell et al., 2019). The at-
 137 mospheric component of E3SM uses a spectral element dynamical core with notable im-
 138 provements in physics and vertical resolution when compared to its predecessor (Rasch
 139 et al., 2019). The ocean component of E3SM, which is the Model for Prediction Across
 140 Scales-Ocean (Petersen et al., 2019), uses a centroidal Voronoi tessellation grid with a z-
 141 star coordinate system in the vertical.

142 For E3SM_LR, we use data from 30 years of a historical simulation covering the
 143 period 1985-2014. This simulation is part of the E3SM project’s contribution to CMIP6.
 144 For further information related to this simulation, see Golaz et al. (2019). For E3SM_HR,
 145 the simulation uses a time-invariant 1950s forcing following the HighResMIP protocol
 146 (Haarsma et al., 2016). Similar to E3SM_LR, we use 30 years of model simulations from
 147 E3SM_HR. For more details regarding the E3SM_HR simulation, see Caldwell et al. (2019).
 148 Besides these coupled simulations, we also use uncoupled ocean and sea ice-only simu-
 149 lations where the ocean and sea-ice models are forced by a data atmosphere based on
 150 the CORE forcing (Large & Yeager, 2009). We use 30 years of the uncoupled simula-
 151 tion at the standard resolution (denoted as E3SM_LR_DA) and 20 years of uncoupled
 152 simulation at the high-resolution (denoted as E3SM_HR_DA).

153 2.3 Calculations

154 We compute the mixed layer heat budget as follows

$$\rho C_p h \frac{\partial T}{\partial t} = -\rho C_p h \bar{V} \cdot \nabla T + Q_{surf} + Q_{vert} \quad (1)$$

155 Here, ρ is the seawater density, C_p is the specific heat capacity ($4000 \text{ J Kg}^{-1} \text{ K}^{-1}$) of
 156 seawater, h is the mixed layer depth, T is the mixed layer-averaged temperature, \bar{V} is
 157 the mixed layer-averaged horizontal velocity vector, Q_{surf} is the net surface heat flux
 158 at the top of the ocean surface and Q_{vert} represents vertical processes at the base of the
 159 mixed layer, including advection and mixing. Q_{surf} is simply estimated as the sum of
 160 incoming shortwave, outgoing longwave, latent and sensible heat fluxes, and corrected
 161 for penetration of shortwave flux at the base of the mixed layer. For observations, the

162 Q_{vert} term is estimated as a 'residual' assuming that the equation is approximately in
 163 balance. Also, for observations, we assume an albedo of 6% and the absorption of short-
 164 wave radiation in the upper-ocean is based on the Jerlov type II scheme (Kara et al., 2005),
 165 which is consistent with the model simulations.

166 Following Jia et al. (2011), the eddy kinetic energy (EKE) in the ocean is computed
 167 as

$$EKE = \frac{1}{2} \frac{g^2}{f^2} \left(\left(\frac{\partial \eta'}{\partial y} \right)^2 + \left(\frac{\partial \eta'}{\partial x} \right)^2 \right) \quad (2)$$

168 Here, g is the acceleration due to gravity, f is the Coriolis parameter, η is the sea sur-
 169 face height and the prime denotes a deviation from the long-term mean.

170 The SWCRE is estimated as the difference between the top-of-atmosphere upwelling
 171 clear-sky shortwave radiation and the top-of-atmosphere upwelling all-sky radiation.

172 3 Results

173 The annual mean SST bias from the CMIP6 multi-model ensemble, shown in Fig.
 174 1A, is consistent with the well-known pattern (Large & Danabasoglu, 2006; Richter, 2015;
 175 Richter et al., 2016). In the tropics and subtropics, we have cold biases in most regions
 176 except near the eastern boundaries, which are characterized by warm SST biases. Sig-
 177 nificant warm biases can also be found in much of the Southern Ocean. The spatial pat-
 178 tern of SST bias in E3SM_LR (Fig. 1B) is largely similar to that in the CMIP6 multi-
 179 model ensemble. However, there are also some notable differences. For instance, the cold
 180 bias in the sub-polar North Atlantic is considerably stronger, which was attributed to
 181 excessive sea ice formation in the Labrador Sea (Golaz et al., 2019). Also, the warm bias
 182 in the Southern Ocean was found to be larger, likely due to an overly aggressive mesoscale
 183 eddy parameterization (Golaz et al., 2019). Compared to E3SM_LR, the mean SST bias
 184 improves considerably in E3SM_HR (Fig. 1C). The most significant improvement is in
 185 the Labrador Sea region due to an improved representation of sea ice and ocean mesoscale
 186 eddies (Caldwell et al., 2019). Biases also improve in the western boundary current re-
 187 gions of the Northwest Pacific and Atlantic, and in the Southern Ocean, likely due to
 188 more realistic eddy activity simulated in those regions (Fig. S1). However, the warm bi-
 189 ases in the eastern boundaries are less affected by an increase in resolution. In fact, the
 190 two most prominent regions of SST bias in E3SM_HR are the regions of warm bias near
 191 the Benguela Current in the Southeast Atlantic and the Subtropical Eastern North Pa-
 192 cific (SENP).

193 We now take a closer look at the SST bias in SENP. The warm SST bias in the CMIP6
 194 multi-model ensemble (Fig. 1D), exceeding several degrees, mainly occurs along the coast
 195 between 20°N and 40°N, and gradually decreases southwestwards. In E3SM_LR (Fig.
 196 1E), the bias along the coast is similar to that in CMIP6. The bias in the offshore re-
 197 gion however is slightly stronger (about 1.5°C) and centered near 120°W and 25°N. Un-
 198 like E3SM_LR, in E3SM_HR (Fig. 1F) the strongest bias, exceeding 2°C, is away from
 199 the coastline and centered near 120°W and 25°N. Note that the offshore bias in E3SM_LR
 200 and E3SM_HR are nearly co-located. Next, to understand the impact of coupling on SST
 201 biases, we consider the mean SST bias in E3SM_LR_DA and E3SM_HR_DA (Fig. S2),
 202 where the ocean is forced by a data atmosphere. The bias improves substantially in many
 203 regions with the warm bias almost disappearing in the subtropical eastern boundary re-
 204 gions. These results probably suggest that the SENP warm bias mainly results from cou-
 205 pling and is less sensitive to an increase in resolution, which leads us to the following ques-
 206 tions: What processes are responsible for the SENP SST bias? Why doesn't an increase
 207 in resolution help improve it?

208 To address these questions, we now examine the observed mixed layer heat bud-
 209 get in detail to determine the various processes responsible for the SST bias in the SENP.
 210 The observed climatology of various terms, averaged over the peak warm bias region of
 211 125°W - 120°W and 25°N - 30°N , is shown in Fig. 2A. Note that the heat budget is not
 212 very sensitive to the exact area over which the terms are averaged. The primary balance
 213 is between the net surface heat flux and vertical advection and mixing with relatively
 214 less contribution from horizontal advection. We next consider the heat budget in the un-
 215 coupled E3SM_LR_DA (solid lines in Fig. 2A). To verify that our computation of the
 216 budget in the model is correct, we estimated the temperature tendency term as the sum
 217 of other terms in the heat budget equation besides directly calculating it using the mixed
 218 layer-averaged temperature. The close correspondence between the two suggests that our
 219 estimates of the various terms in the budget equation are reasonably accurate. Even in
 220 E3SM_LR_DA, the balance is mainly between surface fluxes and vertical processes as in
 221 observations but with small differences. For instance, the heating of the mixed layer from
 222 the net surface heat flux term is slightly stronger in observations than in E3SM_LR_DA
 223 with maximum values of $1.4\text{e-}6\text{ }^{\circ}\text{C s}^{-1}$ and $1.1\text{e-}6\text{ }^{\circ}\text{C s}^{-1}$ respectively. Also, in observa-
 224 tions, the vertical processes tend to cool the mixed layer the most in July. On the other
 225 hand, in E3SM_LR_DA, the maximum cooling from vertical processes is shifted slightly
 226 to August. Despite this, the budget from E3SM_LR_DA is broadly consistent with the
 227 observed budget and, consequently, we use the E3SM_LR_DA as the baseline for com-
 228 parison in the rest of the paper.

229 In both E3SM_LR (Fig. 2B) and E3SM_HR (Fig. 2C), the surface fluxes tend to
 230 heat the mixed layer more than in E3SM_LR_DA (Fig. 2A). To understand this further,
 231 we separate the various terms constituting the net surface heat flux. While the short-
 232 wave flux peaks at about 216 W m^{-2} in E3SM_LR_DA (Fig. 2D), its maximum is nearly
 233 50 W m^{-2} larger in E3SM_LR (Fig. 2E) and E3SM_HR (Fig. 2F). Despite a stronger
 234 longwave flux out of the ocean, the net effect of radiative fluxes is to heat up the mixed
 235 layer more strongly in E3SM_LR and E3SM_HR. While the mean tendency due to ra-
 236 diative fluxes is $1.25\text{e-}6\text{ }^{\circ}\text{C s}^{-1}$ in E3SM_LR_DA, its value in E3SM_LR and E3SM_HR
 237 are $1.75\text{e-}6\text{ }^{\circ}\text{C s}^{-1}$ and $2.1\text{e-}6\text{ }^{\circ}\text{C s}^{-1}$ respectively. The excess shortwave flux in the model
 238 is related to the poor simulation of marine stratocumulus clouds (Golaz et al., 2019; Cald-
 239 well et al., 2019), a problem affecting most coupled models (Stockdale et al., 1994; C-
 240 C. Ma et al., 1996; Richter, 2015; Richter et al., 2016). The latent and sensible heat fluxes
 241 tend to cool the ocean more in E3SM_LR and E3SM_HR when compared to E3SM_LR_DA.
 242 The mean tendency due to these in E3SM_LR and E3SM_HR are $-1.1\text{e-}6\text{ }^{\circ}\text{C s}^{-1}$ and $-$
 243 $1.5\text{e-}6\text{ }^{\circ}\text{C s}^{-1}$ respectively, and are stronger than that in E3SM_LR_DA ($-0.9\text{ e-}6\text{ }^{\circ}\text{C s}^{-1}$).
 244 This is especially the case during Boreal Fall. To understand the bias in surface turbu-
 245 lent fluxes, we examine the change in mean surface winds. Compared to E3SM_LR_DA
 246 (Fig. 2G), the circulation is weaker in both E3SM_LR (Fig. 2H) and E3SM_HR (Fig.
 247 2I). Thus, we suggest that the excessive latent and sensible heat flux out of the ocean
 248 in the coupled simulations is likely due to a warmer ocean surface.

249 When considering the tendency due to horizontal advection, the contribution is more
 250 positive in both E3SM_LR (Fig. 2B) and E3SM_HR (Fig. 2C) compared to E3SM_LR_DA
 251 (Fig. 2A), especially between June and August. While the tendency remains below 0.03e-
 252 $6\text{ }^{\circ}\text{C s}^{-1}$ in E3SM_LR_DA, the maximum value reaches $0.4\text{e-}6\text{ }^{\circ}\text{C s}^{-1}$ and $1.1\text{e-}6\text{ }^{\circ}\text{C s}^{-1}$
 253 in E3SM_LR and E3SM_HR respectively. This increase is caused by errors in surface winds.
 254 As seen earlier, the surface winds are weaker in the coupled simulations (Figs. 2H and
 255 2I) and it appears that there is an anomalous convergence over the region of warm bias.
 256 This is substantiated by considering the differences in upper-ocean convergence in E3SM_LR
 257 relative to E3SM_LR_DA (Fig. 3A). Strong negative values are found over the region 130°W -
 258 120°W and 23°N - 33°N , which is the main region of warm bias. Averaged over this re-
 259 gion, the convergence decreases to nearly $-3.5\text{e-}8\text{ s}^{-1}$ in E3SM_LR and $-4.5\text{e-}8\text{ s}^{-1}$ in E3SM_HR,
 260 indicating enhanced upper-ocean convergence compared to the uncoupled simulation (Fig.
 261 3B). The seasonal timing of the increase in convergence is also consistent with that in

the tendency due to horizontal advection (Figs. 2B and 2C). This suggests that errors in upper-ocean convergence caused by those in surface winds are mainly responsible for the anomalous horizontal advection in E3SM_LR and E3SM_HR.

Finally, vertical processes tend to cool the mixed layer more strongly in E3SM_LR (Fig. 2B) and E3SM_HR (Fig. 2C), compared to the uncoupled E3SM_LR_DA (Fig. 2A). To understand this, let us consider vertical mixing for instance. The contribution from vertical mixing to temperature change is proportional to $\kappa \frac{\partial T}{\partial z}$, where κ is the vertical thermal eddy diffusivity and $\frac{\partial T}{\partial z}$ is the vertical temperature gradient. Compared to E3SM_LR_DA, the maximum magnitude of κ decreases by nearly $0.005 \text{ m}^2 \text{ s}^{-1}$ in E3SM_LR (Fig. 3C), indicating a reduction in mixing strength in the coupled simulation. On the other hand, at a depth of 30-40 m, the difference in the vertical temperature gradient is nearly $-0.15 \text{ }^\circ\text{C}$ between E3SM_LR and E3SM_LR_DA, indicating a significantly larger thermal stratification in the coupled simulation (Fig. 3D). Also, the maximum difference in the vertical temperature gradient occurs around September and is consistent with the bias in the SST seasonal cycle (Fig. S3). Thus, the vertical mixing process tends to cool the mixed layer more in E3SM_LR due to a stronger vertical temperature gradient induced by a warmer SST.

When going from a relatively coarse to a high resolution in the fully-coupled E3SM, we found that while the SST bias improves in many regions, the warm bias in the SENP is largely unaffected. Though surprising, these results are consistent with a previous study using a General Circulation Model configured at a similar eddy-resolving horizontal resolution (Zheng et al., 2010). Albeit in a different region, some other studies showed that an increase in resolution can lead to an improvement in the warm bias. For instance, J. Ma et al. (2019) show that an increase in resolution can potentially reduce the bias through an improved simulation of coastal upwelling. Even in our simulations using E3SM, the representation of upwelling processes along the coast improves in E3SM_HR compared to E3SM_LR (Fig. S4). The thermocline rises more sharply near the coast in E3SM_HR causing a reduction of the near-shore SST bias in the high-resolution simulation. Despite this, the offshore SST bias is stronger in E3SM_HR compared to E3SM_LR (Fig. 1).

To put these results based on E3SM in perspective, we evaluated the SST bias from the HighResMIP suite of models. Consistent with results from E3SM, in the low-resolution configuration of the models, the multi-model mean SENP bias, exceeding several degrees in magnitude, is concentrated along the coastline between 25°N and 40°N (Fig. 4A). On the other hand, the coastal SENP SST bias is substantially reduced in the high-resolution configuration of these models (Fig. 4B). Also, consistent with E3SM, the offshore bias in the high-resolution configuration is larger than that in the low-resolution configuration. The peak warm bias is about 1°C and is centered at approximately 120°W and 25°N . Further, the warm bias in the high-resolution configuration also extends southwestwards. Thus, the lack of significant improvement in the SENP SST bias with an increase in model resolution is not native to E3SM alone but is also seen in other models.

A possible reason for the SENP SST bias that we suggested previously was the weaker anticyclonic surface wind circulation in the fully-coupled simulations, suggestive of a weaker subtropical high in the coupled simulations relative to observations (Fig. 2). An anomalous southerly wind can simultaneously reduce upwelling along the coast and hinder the offshore Ekman transport of cold water. To understand this further, we plotted the meridional wind stress bias against the SST bias, averaged over the region between 130°W - 115°W and 20°N - 30°N , from CMIP6 models (Fig. 4C). In general, models with larger surface wind biases also tend to be models with stronger SST biases. The correlation coefficient is about 0.47, significant at the 95% level. Further, to understand the relative significance of the bias in surface winds, we plotted errors in shortwave cloud forcing (SWCRE) against the SST bias from the same models (Fig. 4D). The correlation, significant at more than 90%, is about 0.31. Also, the biases in SWCRE and meridional winds are uncorrelated (about 0.13). These results suggest that inter-model differences in SST biases in

315 the SENP region are related more to the biases in surface winds than to the biases in
 316 stratus cloud in the simulations. While biases in surface winds can lead to those in SSTs,
 317 warm SSTs may induce wind convergence and reinforce the initial wind bias through a
 318 positive feedback. To clarify the connection between the wind and SST biases, the cor-
 319 relation between meridional wind and SST averaged over the SENP warm bias region
 320 (130°W - 115°W and 20°N - 30°N) is 0.34 ± 0.06 at zero lag. However, the correlation in-
 321 creases to 0.42 ± 0.05 with winds leading SST by a month, and the correlation drops to
 322 0.09 ± 0.06 vice versa. Based on this, we suggest that SST is mostly responding to the
 323 wind bias, even though the SST anomaly may also play a role in enhancing the wind bias.

324 4 Discussion

325 Although we looked at the surface wind circulation from an annual mean perspec-
 326 tive, seasonal averages (Fig. S5) indicate that the biases are persistent across the var-
 327 ious seasons, especially to the south of 30°N . The anomalous southerly winds in the sub-
 328 tropics likely indicate a weaker subtropical high, which we speculate may in turn be re-
 329 lated to biases in Hadley circulation or remote circulation features with tropical or ex-
 330 tratropical origins in models (Li & Xie, 2014). To further delineate the role of remote
 331 and local processes in the SENP SST error, a promising approach that could be employed
 332 is the use of ‘initial SST tendency’ experiments (Toniazzi et al., 2010; H.-Y. Ma et al.,
 333 2015).

334 Besides the processes examined thus far in the study, one other possibility is the
 335 error in the mixed layer depth. In both E3SM_LR and E3SM_HR, model simulated mixed
 336 layers are shallower than those in the uncoupled E3SM_LR_DA (Fig. S6), which can then
 337 amplify the bias in the mixed layer-averaged temperature. While the weaker winds can
 338 certainly be a cause, errors in mean precipitation could also contribute to the bias in mixed
 339 layers. In the fully-coupled configuration, the model tends to produce excessive rainfall
 340 along and in the near-shore of the North American west coast (Golaz et al., 2019; Cald-
 341 well et al., 2019). This can subsequently induce errors in the mixed layer through its ef-
 342 fect on upper-ocean salinity stratification. Thus, beyond an accurate representation of
 343 surface winds, improving precipitation processes in coupled climate models could also
 344 be a key to alleviate the SENP warm SST bias.

345 Overall, our results based on E3SM, HighResMIP, and CMIP6 simulations suggest
 346 common sources of the SENP biases that largely remain in models from coarse resolu-
 347 tion to relatively high resolution. This emphasizes the need to improve coupled model
 348 skill through improvements in physics parameterizations and develop metrics that bet-
 349 ter relate the SENP bias to its sources to guide model development.

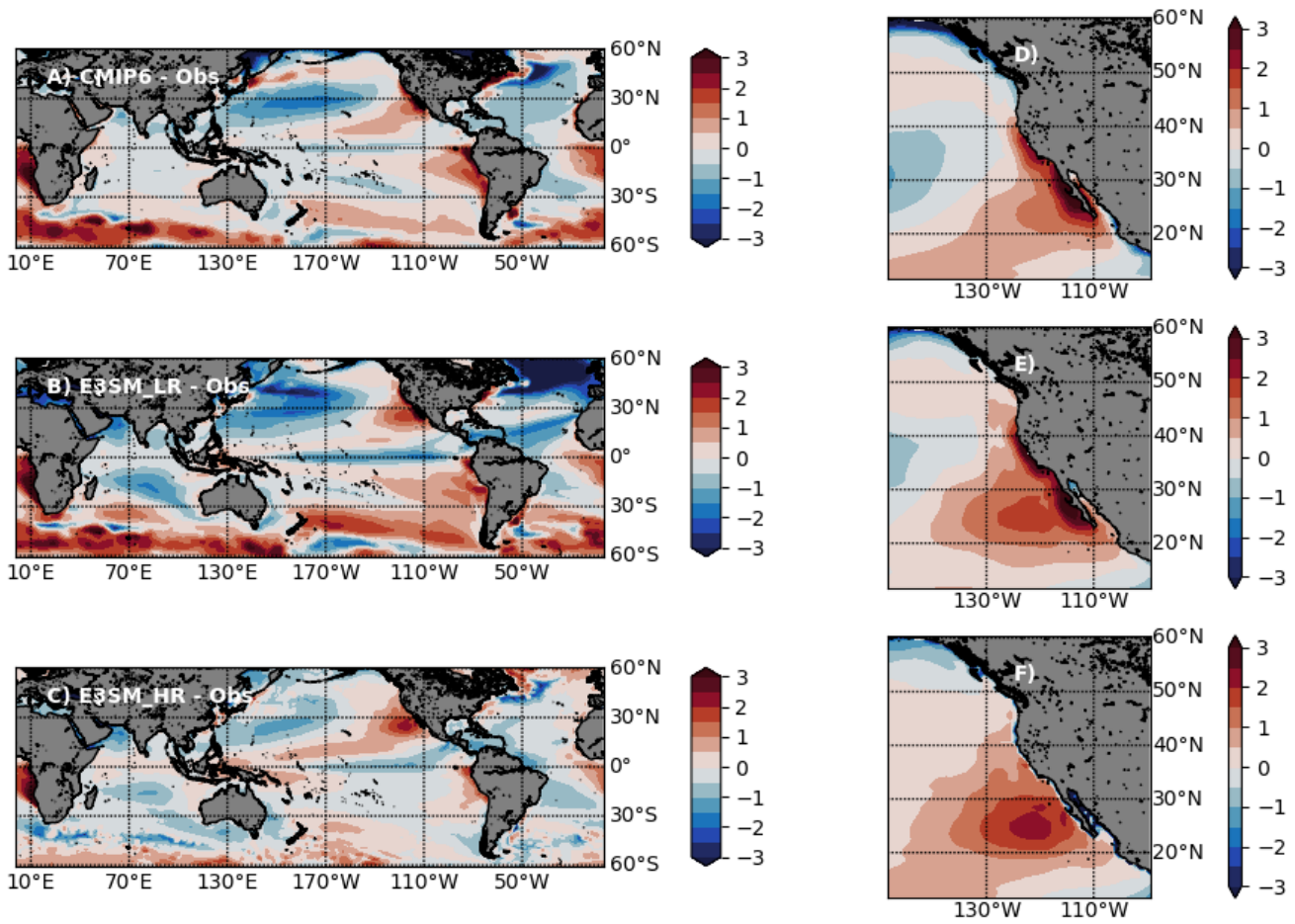


Figure 1. The annual mean SST bias ($^{\circ}\text{C}$) in A) CMIP6, B) E3SM_LR and C) E3SM_HR. D-F) As in A-C but for the SENP region. The bias is computed with respect to the NOAA OI SST.

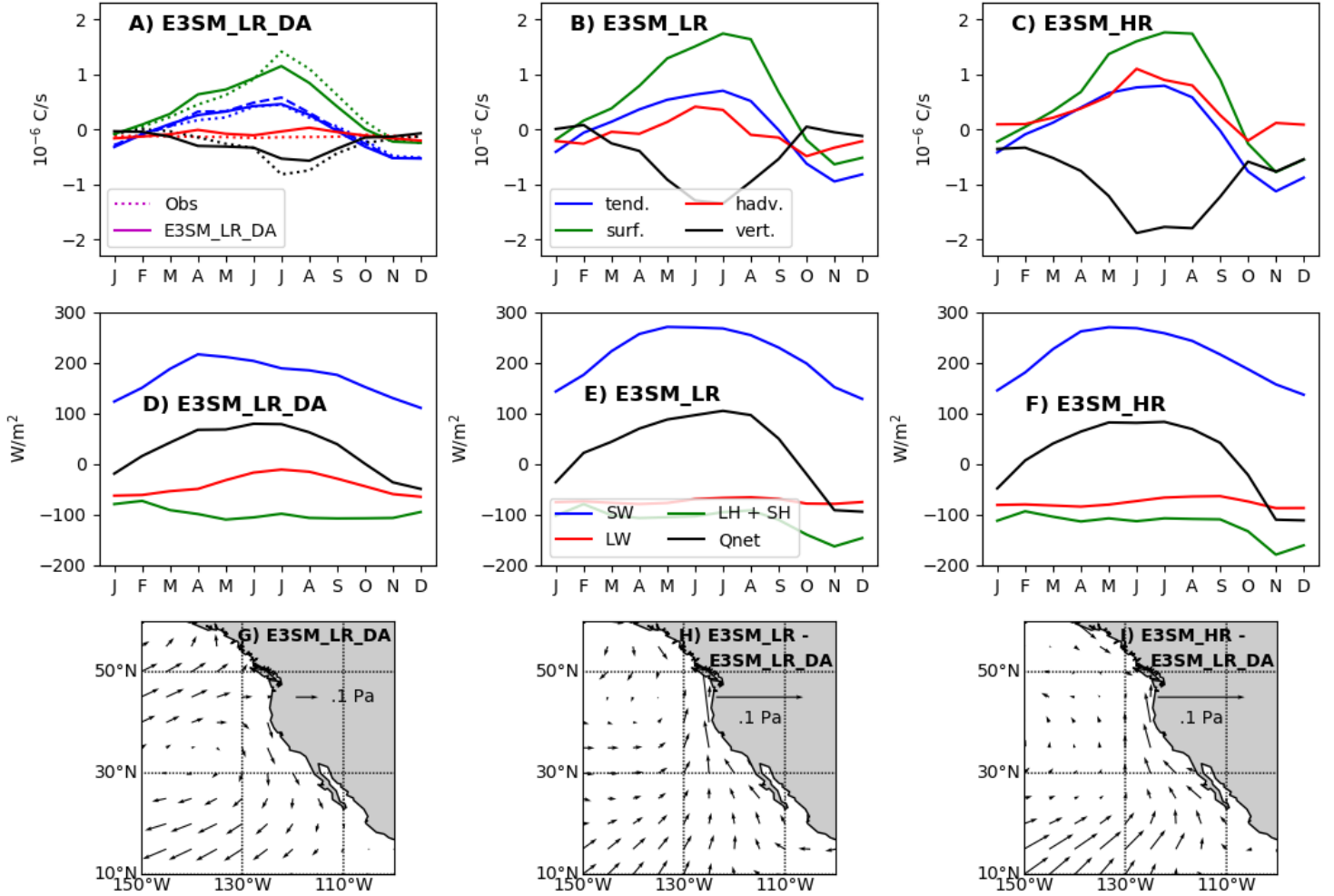


Figure 2. The climatology of various terms contributing to the mixed layer heat budget in A) E3SM_LR_DA, B) E3SM_LR and C) E3SM_HR. The time tendency of mixed layer-averaged temperature is in blue, the tendency due to net surface heat flux is in green, the tendency due to horizontal advection is in red, and the tendency due to vertical processes is in black. In panel A, the budget terms from Observations are shown as dotted lines. In panel B, the time tendency of mixed layer-averaged temperature, estimated indirectly as a sum of other terms of the heat budget equation, is shown as a blue dashed line. The climatology of terms constituting the net surface heat flux in D) E3SM_LR_DA, E) E3SM_LR, and F) E3SM_HR. The net heat flux is in magenta, the shortwave flux is in blue, the longwave flux is in red, and the sum of latent and sensible heat fluxes is in green. Positive represents into the ocean and negative indicates out of the ocean. In panels A-F, each term is averaged over the region of 125°W - 120°W and 25°N - 30°N and has units of W m^{-2} . G) The annual mean surface circulation, represented by wind stress (N m^{-2}), in E3SM_LR_DA. The anomalous annual mean surface winds in H) E3SM_LR and I) E3SM_HR.

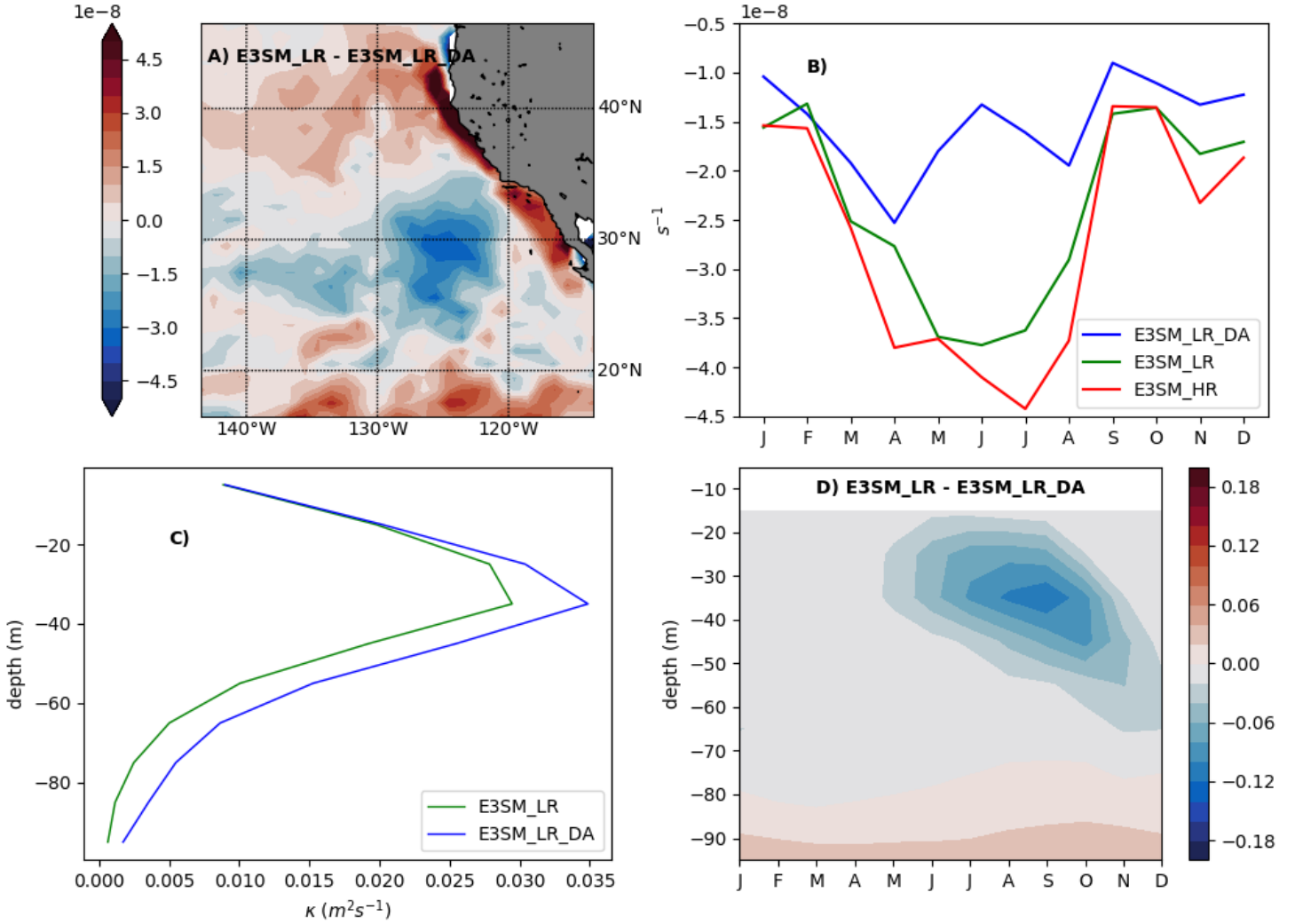


Figure 3. A) The difference in upper-ocean mean convergence (s^{-1}), based on mixed layer-averaged currents, between E3SM_LR and E3SM_LR_DA. Negative values indicate an increase in convergence. B) The climatological seasonal cycle of upper-ocean convergence, averaged over the region of $125^{\circ}W$ - $120^{\circ}W$ and $25^{\circ}N$ - $30^{\circ}N$, in E3SM_LR_DA (blue), E3SM_LR (green) and E3SM_HR (red). C) Annual mean profiles of vertical thermal eddy diffusivity (κ , m^2s^{-1}), averaged over the region of $125^{\circ}W$ - $120^{\circ}W$ and $25^{\circ}N$ - $30^{\circ}N$, in E3SM_LR_DA (blue) and E3SM_LR (green). D) Difference in annual mean vertical temperature gradients ($\frac{\partial T}{\partial z}$, $^{\circ}Cs^{-1}$) between E3SM_LR and E3SM_LR_DA. Negative values indicate an enhancement of temperature stratification.

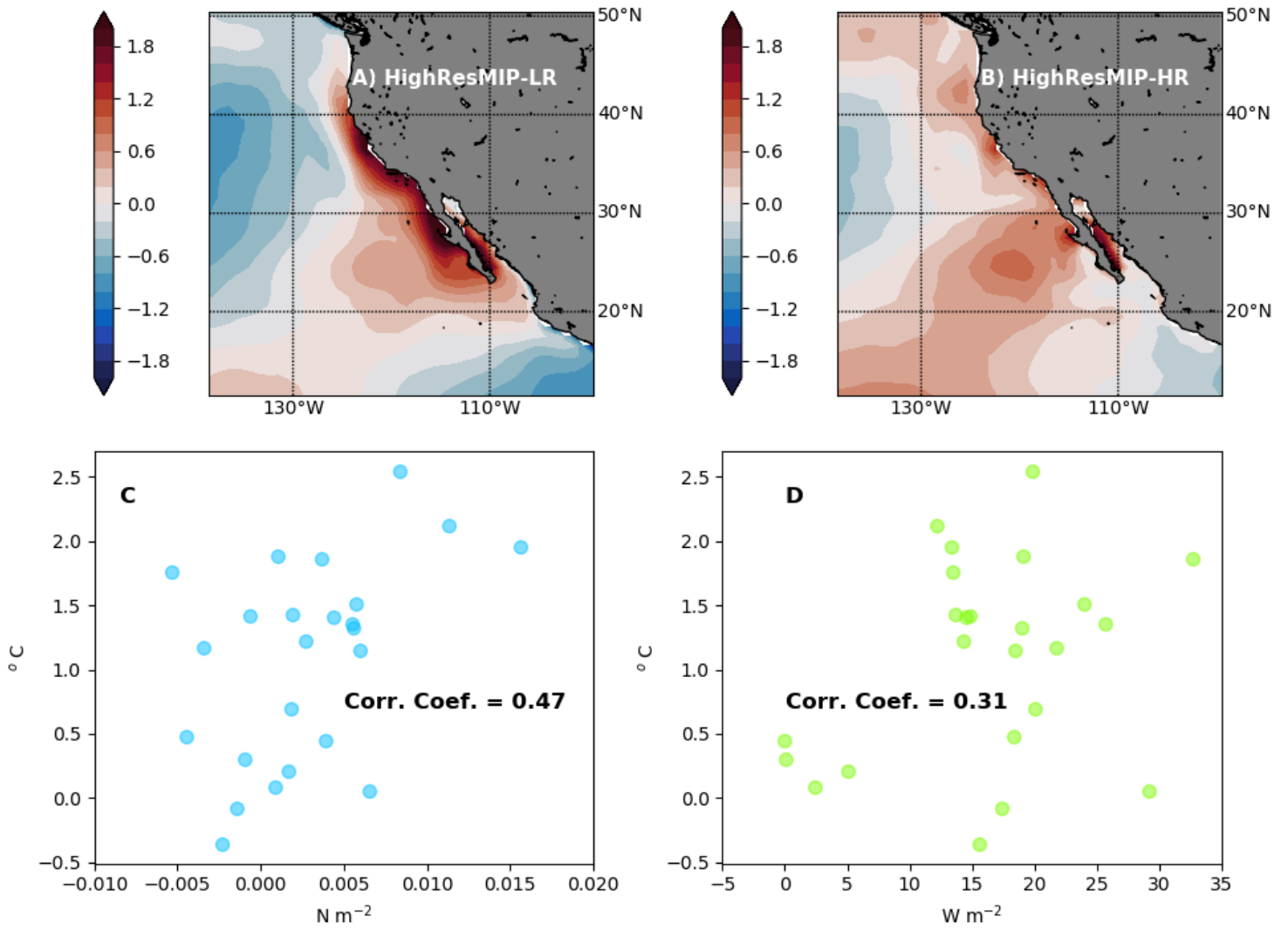


Figure 4. The annual mean SST bias ($^{\circ}\text{C}$) in A) low-resolution and B) high-resolution configurations of 8 HighResMIP models. Anomalous SST (y-axis) plotted against C) anomalous meridional windstress (x-axis) and D) anomalous SWCRE (x-axis), averaged over the region 130°W - 115°W and 20°N - 30°N , for 24 CMIP6 models. The respective correlation coefficients are also indicated in panels C and D.

Acknowledgments

K.B., L.V.R., L.R.L. and M.V. acknowledge support from the E3SM project, funded by the U.S. Department of Energy, Office of Science, Office of Biological and Environmental Research (BER). The Pacific Northwest National Laboratory is operated for DOE by Battelle Memorial Institute under contract DE-AC05-76RL01830. The sources for various data used in this study are as follows: NOAA monthly mean SST - <https://ps1.noaa.gov/data/gridded/data.noaa.oisst.v2.highres.html>, ECMWF OARS5 monthly mean meridional wind stress - <https://www.ecmwf.int/en/forecasts/dataset/ocean-reanalysis-system-5>, CERES-EBAF Ed4.0 observations of shortwave cloud radiation - <https://ceres.larc.nasa.gov>, OAFflux monthly mean air-sea fluxes - <http://oaf Flux.whoii.edu>, Argo gridded temperature and salinity data - http://apdrc.soest.hawaii.edu/projects/Argo/data/gridded/On_standard_levels/index-1.html, OSCAR 5-day mean surface ocean currents - https://podaac.jpl.nasa.gov/dataset/OSCAR.L4_OC.third-deg, AVISO monthly mean multi-satellite merged sea level anomalies - <https://www.aviso.altimetry.fr/en/home.html>, CMIP6 and HighResMIP data - <https://esgf-node.llnl.gov/projects/esgf-llnl/>.

References

- Ashfaq, M., Skinner, C. B., & Diffenbaugh, N. S. (2011). Influence of sst biases on future climate change projections. *Climate Dynamics*, *36*(7-8), 1303–1319.
- Bakun, A., & Nelson, C. S. (1991). The seasonal cycle of wind-stress curl in subtropical eastern boundary current regions. *Journal of Physical Oceanography*, *21*(12), 1815–1834.
- Balaguru, K., Chang, P., Saravanan, R., & Jang, C. (2012). The barrier layer of the atlantic warmpool: Formation mechanism and influence on the mean climate. *Tellus A: Dynamic Meteorology and Oceanography*, *64*(1), 18162.
- Caldwell, P. M., Mametjanov, A., Tang, Q., Van Roekel, L. P., Golaz, J.-C., Lin, W., ... others (2019). The doe e3sm coupled model version 1: Description and results at high resolution. *Journal of Advances in Modeling Earth Systems*, *11*(12), 4095–4146.
- Chavez, F. P., & Messié, M. (2009). A comparison of eastern boundary upwelling ecosystems. *Progress in Oceanography*, *83*(1-4), 80–96.
- da Silveira, I. P., Zuidema, P., & Kirtman, B. P. (2019). Fast sst error growth in the southeast pacific ocean: comparison between high and low-resolution ccsm4 retrospective forecasts. *Climate Dynamics*, *53*(9), 5237–5251.
- Dohan, K., & Maximenko, N. (2010). Monitoring ocean currents with satellite sensors. *Oceanography*, *23*(4), 94–103.
- García-Reyes, M., Syde-man, W. J., Schoeman, D. S., Rykaczewski, R. R., Black, B. A., Smit, A. J., & Bograd, S. J. (2015). Under pressure: Climate change, upwelling, and eastern boundary upwelling ecosystems. *Frontiers in Marine Science*, *2*, 109.
- Gent, P. R., Yeager, S. G., Neale, R. B., Levis, S., & Bailey, D. A. (2010). Improvements in a half degree atmosphere/land version of the ccsm. *Climate Dynamics*, *34*(6), 819–833.
- Golaz, J.-C., Caldwell, P. M., Van Roekel, L. P., Petersen, M. R., Tang, Q., Wolfe, J. D., ... others (2019). The doe e3sm coupled model version 1: Overview and evaluation at standard resolution. *Journal of Advances in Modeling Earth Systems*, *11*(7), 2089–2129.
- Haarsma, R. J., Roberts, M. J., Vidale, P. L., Senior, C. A., Bellucci, A., Bao, Q., ... others (2016). High resolution model intercomparison project (highresmip v1. 0) for cmip6. *Geoscientific Model Development*, *9*(11), 4185–4208.
- Harlaß, J., Latif, M., & Park, W. (2018). Alleviating tropical atlantic sector biases in the kiel climate model by enhancing horizontal and vertical atmosphere model resolution: climatology and interannual variability. *Climate Dynamics*,

- 403 50(7), 2605–2635.
- 404 Jia, F., Wu, L., & Qiu, B. (2011). Seasonal modulation of eddy kinetic energy and
405 its formation mechanism in the southeast indian ocean. *Journal of Physical*
406 *Oceanography*, 41(4), 657–665.
- 407 Kara, A. B., Wallcraft, A. J., & Hurlburt, H. E. (2005). A new solar radiation
408 penetration scheme for use in ocean mixed layer studies: An application to
409 the black sea using a fine-resolution hybrid coordinate ocean model (hycom).
410 *Journal of physical oceanography*, 35(1), 13–32.
- 411 Kessler, W. S. (2006). The circulation of the eastern tropical pacific: A review.
412 *Progress in Oceanography*, 69(2-4), 181–217.
- 413 Kurian, J., Li, P., Chang, P., Patricola, C. M., & Small, J. (2021). Impact of the
414 benguela coastal low-level jet on the southeast tropical atlantic sst bias in a
415 regional ocean model. *Climate Dynamics*, 1–28.
- 416 Large, W., & Danabasoglu, G. (2006). Attribution and impacts of upper-ocean bi-
417 ases in ccm3. *Journal of Climate*, 19(11), 2325–2346.
- 418 Large, W., & Yeager, S. (2009). The global climatology of an interannually varying
419 air–sea flux data set. *Climate dynamics*, 33(2-3), 341–364.
- 420 Leung, L. R., Bader, D. C., Taylor, M. A., & McCoy, R. B. (2020). An introduction
421 to the e3sm special collection: Goals, science drivers, development, and analy-
422 sis. *Journal of Advances in Modeling Earth Systems*, 12(11), e2019MS001821.
- 423 Li, G., & Xie, S.-P. (2014). Tropical biases in cmip5 multimodel ensemble: The ex-
424 cessive equatorial pacific cold tongue and double itcz problems. *Journal of Cli-*
425 *mate*, 27(4), 1765–1780.
- 426 Loeb, N. G., Wielicki, B. A., Doelling, D. R., Smith, G. L., Keyes, D. F., Kato, S.,
427 ... Wong, T. (2009). Toward optimal closure of the earth’s top-of-atmosphere
428 radiation budget. *Journal of Climate*, 22(3), 748–766.
- 429 Ma, C.-C., Mechoso, C. R., Robertson, A. W., & Arakawa, A. (1996). Peruvian
430 stratus clouds and the tropical pacific circulation: A coupled ocean-atmosphere
431 gcm study. *Journal of Climate*, 9(7), 1635–1645.
- 432 Ma, H.-Y., Chuang, C., Klein, S., Lo, M.-H., Zhang, Y., Xie, S., ... Phillips, T.
433 (2015). An improved hindcast approach for evaluation and diagnosis of physi-
434 cal processes in global climate models. *Journal of Advances in Modeling Earth*
435 *Systems*, 7(4), 1810–1827.
- 436 Ma, J., Xu, S., & Wang, B. (2019). Warm bias of sea surface temperature in eastern
437 boundary current regions—a study of effects of horizontal resolution in cesm.
438 *Ocean Dynamics*, 69(8), 939–954.
- 439 Meinshausen, M., Vogel, E., Nauels, A., Lorbacher, K., Meinshausen, N., Etheridge,
440 D. M., ... others (2017). Historical greenhouse gas concentrations for climate
441 modelling (cmip6). *Geoscientific Model Development*, 10(5), 2057–2116.
- 442 Petersen, M. R., Asay-Davis, X. S., Berres, A. S., Chen, Q., Feige, N., Hoffman,
443 M. J., ... others (2019). An evaluation of the ocean and sea ice climate
444 of e3sm using mpas and interannual core-ii forcing. *Journal of Advances in*
445 *Modeling Earth Systems*, 11(5), 1438–1458.
- 446 Rasch, P., Xie, S., Ma, P.-L., Lin, W., Wang, H., Tang, Q., ... others (2019). An
447 overview of the atmospheric component of the energy exascale earth system
448 model. *Journal of Advances in Modeling Earth Systems*, 11(8), 2377–2411.
- 449 Reynolds, R. W., Rayner, N. A., Smith, T. M., Stokes, D. C., & Wang, W. (2002).
450 An improved in situ and satellite sst analysis for climate. *Journal of climate*,
451 15(13), 1609–1625.
- 452 Richter, I. (2015). Climate model biases in the eastern tropical oceans: causes,
453 impacts and ways forward. *Wiley Interdisciplinary Reviews: Climate Change*,
454 6(3), 345–358.
- 455 Richter, I., Doi, T., Chang, P., Xu, Z., Kataoka, T., Tozuka, T., ... De Szoeke, S. P.
456 (2016). An overview of coupled gcm biases in the tropics. In *Indo-pacific*
457 *climate variability and predictability* (pp. 213–263). World Scientific.

- 458 Richter, I., & Xie, S.-P. (2008). On the origin of equatorial atlantic biases in coupled
 459 general circulation models. *Climate Dynamics*, *31*(5), 587–598.
- 460 Roemmich, D., Johnson, G. C., Riser, S., Davis, R., Gilson, J., Owens, W. B., ...
 461 Ignaszewski, M. (2009). The argo program: Observing the global ocean with
 462 profiling floats. *Oceanography*, *22*(2), 34–43.
- 463 Small, R. J., Curchitser, E., Hedstrom, K., Kauffman, B., & Large, W. G. (2015).
 464 The benguela upwelling system: Quantifying the sensitivity to resolution and
 465 coastal wind representation in a global climate model. *Journal of Climate*,
 466 *28*(23), 9409–9432.
- 467 Stockdale, T., Latif, M., Burgers, G., & Wolff, J.-O. (1994). Some sensitivities of a
 468 coupled ocean-atmosphere gcm. *Tellus A*, *46*(4), 367–380.
- 469 Toniazzo, T., Mechoso, C. R., Shaffrey, L. C., & Slingo, J. M. (2010). Upper-
 470 ocean heat budget and ocean eddy transport in the south-east pacific in a
 471 high-resolution coupled model. *Climate dynamics*, *35*(7-8), 1309–1329.
- 472 Xie, S.-P., Miyama, T., Wang, Y., Xu, H., De Szoek, S. P., Small, R. J. O., ...
 473 Awaji, T. (2007). A regional ocean-atmosphere model for eastern pacific cli-
 474 mate: Toward reducing tropical biases. *Journal of Climate*, *20*(8), 1504–1522.
- 475 Xu, Z., Chang, P., Richter, I., & Tang, G. (2014). Diagnosing southeast tropical atl-
 476 antic sst and ocean circulation biases in the cmip5 ensemble. *Climate dynam-
 477 ics*, *43*(11), 3123–3145.
- 478 Xu, Z., Li, M., Patricola, C. M., & Chang, P. (2014). Oceanic origin of southeast
 479 tropical atlantic biases. *Climate dynamics*, *43*(11), 2915–2930.
- 480 Yu, L., & Weller, R. A. (2007). Objectively analyzed air-sea heat fluxes for the
 481 global ice-free oceans (1981–2005). *Bulletin of the American Meteorological So-
 482 ciety*, *88*(4), 527–540.
- 483 Zheng, Y., Kiladis, G. N., Shinoda, T., Metzger, E. J., Hurlburt, H. E., Lin, J., &
 484 Giese, B. S. (2010). Upper-ocean processes under the stratus cloud deck in the
 485 southeast pacific ocean. *Journal of physical oceanography*, *40*(1), 103–120.
- 486 Zheng, Y., Shinoda, T., Lin, J.-L., & Kiladis, G. N. (2011). Sea surface temper-
 487 ature biases under the stratus cloud deck in the southeast pacific ocean in
 488 19 ipcc ar4 coupled general circulation models. *Journal of Climate*, *24*(15),
 489 4139–4164.
- 490 Zuidema, P., Chang, P., Medeiros, B., Kirtman, B. P., Mechoso, R., Schneider,
 491 E. K., ... others (2016). Challenges and prospects for reducing coupled
 492 climate model sst biases in the eastern tropical atlantic and pacific oceans:
 493 The us clivar eastern tropical oceans synthesis working group. *Bulletin of the
 494 American Meteorological Society*, *97*(12), 2305–2328.
- 495 Zuo, H., Balmaseda, M. A., Tietsche, S., Mogensen, K., & Mayer, M. (2019). The
 496 ecmwf operational ensemble reanalysis-analysis system for ocean and sea ice: a
 497 description of the system and assessment. *Ocean science*, *15*(3), 779–808.